The Surface and Solution Properties of Dihexadecyl Dimethylammonium Bromide

I. Tucker,*,† J. Penfold,‡ R. K. Thomas,§ I. Grillo,|| J. G. Barker,⊥ and D. F. R. Mildner⊥

Unilever Research and Development Laboratory, Port Sunlight, Quarry Road East, Bebington, Wirral, ISIS, STFC, Rutherford Appleton Laboratory, Chilton, Didcot, OXON, Physical and Theoretical Chemistry Laboratory, Oxford University, South Parks Road, Oxford, Institute Laue-Langevin, 6 Jules Horowitz, F-38042 Grenoble, Cedex 09, France, and National Institute of Science & Technology, Gaithersberg, Maryland

Received November 1, 2007. Revised Manuscript Received March 15, 2008

The surface adsorption behavior and solution aggregate microstructure of the dichain cationic surfactant dihexadecyl dimethylammonium bromide (DHDAB) have been studied using small angle neutron scattering (SANS), light scattering, neutron reflectivity (NR), and surface tension (ST). Using a combination of surface tension and neutron reflectivity, the DHDAB equilibrium surface excess at saturation adsorption has been measured as $2.60 \pm 0.05 \times 10^{-10}$ mol·cm^{-2}. The values obtained by both methods are in good agreement and are consistent with the values reported for other dialkyl chain surfactants. The critical aggregation concentration (CAC) values obtained from both methods (NR and ST) are also in good agreement, with a mean value for the CAC of $4 \pm 2 \times 10^{-5}$ M. The surface equilibrium is relatively slow, and this is attributed to monomer depletion in the near surface region, as a consequence of the long monomer residence times in the surfactant aggregates. The solution aggregate morphology has been determined using a combination of SANS, dynamic light scattering (DLS), cryogenic transmission electron microscopy (CryoTEM), and ultrasmall angle neutron scattering (USANS). Within the concentration range 1.5−80 mM, the aggregates are in the form of bilamellar vesicles with a lamellar "*d*-spacing" of the order of 900 Å. The vesicles are relatively polydisperse with a particle size in the range 2000−4000 Å. Above 80 mM, the bilamellar vesicles coexist with an additional L_β lamellar phase.

1. Introduction

Dichain cationic surfactants are an important class of surfactants which are widely used in many applications in home and personal care products and in lubricants. They are generally derived from naturally occurring vegetable or animal fats whose hydrocarbon chains vary in length from dodecyl to octadecyl. Synthetic quaternary ammonium salts of dialkyl dimethylammonium bromide surfactants are easily synthesized in their pure forms. There have been a number of studies of both the dodecyl and octadecyl versions of these dialkyl dimethylammonium bromide surfactants; however, the dihexadecyl form has received much less attention. In this paper, we aim to address this deficiency and are concerned with determining both the surface and solution behavior of this surfactant. Furthermore, it provides an important input into a much wider study concerning the surface and solution behavior of dihexadecyl dimethylammonium bromide (DHDAB) nonionic surfactant mixtures.[1–3]

There are several recent reports concerning the phase behavior of a range of dialkyl chain cationic surfactants.[4–8] The most extensive reports on phase behavior in such systems are by Dubois and Zemb,[4] Zemb et al.,[5] Haas et al.,[6] Brady et al.,[7] and Caboi and Monduzzi.[8] Although Haas et al. have performed some limited surface tension (ST) studies,[6] there is almost nothing concerning the interfacial properties of DHDAB, apart from some preliminary measurements by Penfold et al.[9] on the related system diheptadecyl-ether dimethylammonium chloride. The measurements made on concentrated solutions, mostly on di-C_{12}DAB or di-C_{18}DAB, show the presence of a lamellar phase, liposomes, and higher order morphologies. At lower concentrations (<1 wt % (∼10−20 mM)), the experimental evidence suggests that the aggregates are mainly micellar, with some evidence for dilute lamellar phase dispersions.[5] The lamellar phase region exhibits a L_β to L_α transition in the temperature range 20−50 °C for di-C_{12} to di-C_{16} surfactants, characteristic of a solidlike to fluidlike transition.[4] Furthermore, the multilamellar vesicle or liposomal phase is often induced by shear.[10] Although there are several articles which feature studies of the di-C_{12} cationic surfactant, DDAB, there is very little information in the literature that is of direct relevance to DHDAB. Specific mention of the DHDAB cationic surfactant was made by Haas et al.,[6] who produced an initial phase diagram, and by Brady et al.,[7] who discussed the phase behavior in terms of a lamellar phase dispersion and reported a L_β to L_α transition temperature at 40 °C. Dubois and Zemb[4] discussed the related surfactant di-C_{16} acetate and reported evidence for an isotropic and L_3 phase at low surfactant concentrations. Radlinska et al.[11] have shown rather unusual solution behavior in the di-C_{12} system with acetate as the counterion. At higher surfactant concentrations (1−5 wt %),

† Unilever Research and Development Laboratory.
‡ Rutherford Appleton Laboratory.
§ Oxford University.
|| Institute Laue-Langevin.
⊥ National Institute of Science & Technology.

(1) Penfold, J.; Tucker, I.; Staples, E.; Thomas, R. K. *Langmuir* **2004**, *20*, 1269.
(2) Tucker, I. M. DPhil Thesis, University of Oxford, 2007.
(3) Penfold, J.; Staples, E.; Ugazio, S.; Tucker, I.; Soubiran, L.; Hubbard, J.; Noro, M.; O'Malley, B.; Ferrante, A.; Ford, G.; Buron, H. *J. Phys. Chem. B* **2005**, *109*, 276.
(4) Dubois, M.; Zemb, T. *Langmuir* **1991**, *7*, 1357.
(5) Zemb, T.; Gazeau, D.; Dubois, M.; Gulik-Krzywicki, T. *Europhys. Lett.* **1993**, *21*, 759.
(6) Haas, S.; Hoffmann, H.; Thunig, C.; Hoinkis, E. *Colloid Polym. Sci.* **1999**, *277*, 856.
(7) Brady, J. E.; Evans, D. F.; Warr, G. G.; Grieser, F.; Ninham, B. W. *J. Phys. Chem.* **1986**, *90*, 1853.
(8) Caboi, F.; Monduzzi, M. *Langmuir* **1996**, *12*, 3548.
(9) Penfold, J.; Staples, E.; Tucker, I.; Soubiran, L.; Creeth, A.; Hubbard, J. *Phys. Chem. Chem. Phys.* **2000**, *2*, 5230.
(10) Diat, O.; Roux, D.; Nallet, F. *J. Phys. II* **1993**, *3*, 1427.
(11) Radlinska, E. Z.; Zemb, T. N.; Dabliez, J.-P.; Ninham, B. W. *Langmuir* **1993**, *9*, 2844.

10.1021/la703415m CCC: $40.75
Published on Web 06/04/2008

McGillivray et al.[12] have used neutron reflectivity to reveal the highly ordered lamellar-like structures that exist at the air−solution and solid−solution interfaces for a range of different dialkyl chain cationic surfactants from di-C_8DAB to DHDAB. Haas et al.[6] and Hass and Hoffmann[13] investigated the entire phase space of these dialkyl chain DAB surfactants. However, they reported the presence of crystals below 40 °C in the di-C_{16} surfactant, and in light of the current study this suggests that their samples were not adequately dispersed. Feitosa et al.[14] have recently reported the existence of lamellar vesicles and tubules in the di-C_{18} DAB systems, determined using rapid freezing electron microscopy, and prior to freezing they manipulated the vesicle size using a supporting electrolyte. Proverbio et al.[15] and Soltero et al.[16] have studied the mixing and solution behavior of di-C_{12}DAB alone and in mixtures with C_{12}TAB in dilute solution, using optical texture fluorescence and conductivity. They reported the presence of vesicles and a critical aggregation concentration (CAC) for di-C_{12}DAB of $5 \pm 3 \times 10^{-5}$ M. Cocquyt et al.[17] studied the melting transitions in di-C_{18}DAB using differential scanning calorimetry (DSC). They observed two transitions at 36 and 44 °C, which were not separately identified.

2. Experimental Details

Protonated DHDAB was obtained from Fluka (Sigma-Aldrich) Chemicals (>98% purity) and was recrystallized twice from ethyl acetate. Chain deuterated DHDAB was synthesized by Dr. R. K. Thomas, Physical and Theoretical Chemistry Laboratory, University of Oxford. The purity of the deuterated surfactant was greater than 98%, verified by both thin layer chromatography and neutron reflectivity, and the levels of deuteration were confirmed by NMR.

2.1. Sample Preparation. Procedures used in the preparation of dilute dispersions were similar to those described by Haas et al.[6] Dilute solutions (up to and including 80 mM) were prepared volumetrically by dispersing a known mass of surfactant in a preset volume of heavy water, D_2O, using elevated temperature to melt the surfactant and mild shaking to disperse the material. Further treatments such as vigorous mixing including sonnication were not required to produce stable, reproducible dispersions. (As part of initial studies in defining a reproducible preparation route, sonication was also applied at elevated temperature but was found to have no effect on the format of the dispersion which ultimately formed and was consequently dropped from subsequent preparations.) Solution optical texture and the absence of crystals or undispersed powder were used as a guide to ensure complete dissolution. However, for higher concentrations (80 mM and above), mild stirring does not give good mixing and a new procedure was developed. Surfactant and D_2O were weighed into a Luer-Lok syringe connected to a second syringe via a nosepiece comprising a junction and two back-to-back Luer female connections. The air was expelled by partially unscrewing one of the nose-ends and carefully closing the piston so as to expel the air. The joint was then reclosed, the syringes were heated to 80 °C for 30 min, and the samples were mixed by exchanging surfactant from one chamber to the other several times. When mixed, the solution was allowed to cool. For the small angle neutron scattering (SANS) measurements, protonated DHDAB was prepared in D_2O to provide optimal scattering contrast. For the surface tension measurements, only the protonated surfactants were used. For the neutron reflectivity measurements, the chain deuterated analogue of DHDAB was used and solutions were prepared in a mixture of 8.9 wt % D_2O in H_2O, null reflecting water (NRW).

Detailed long-term solution stability studies had shown that the Krafft point in this system was 28 °C. This was also confirmed by DSC measurements (see Figure 2 in section 5 of the Supporting Information). As this is the first in a series of papers exploring the relationship between the surface and solution phase behavior of DHDAB in mixtures with nonionic surfactants with 6 and 12 ethylene oxide groups, all measurements were performed at 30 °C in order to avoid complications with the $C_{12}EO_6$ cloud point in subsequent studies. In all cases, the solutions were not allowed to cool below this temperature once dissolution had taken place. Solutions were prepared and placed on long-term storage at this temperature for in excess of 24 months. During this period, no colloidal instability was observed.

2.2. Optical Texture. Using an adaptation of the methods of Zemb et al. [5] and Haas et al.,[6] the optical texture was recorded on a scale from turbid to clear, by visual inspection of solutions left to stand at temperatures between 30 and 60 °C for at least 4 h. No further evolution in the optical texture occurred after 24 h. Samples were viewed between crossed polars to check for anisotropic domains, and for any birefringence.

2.3. Surface Tension. The surface tension measurements were performed using a Kruss K1OST and a Kruss K1OT tensiometer[18] at a temperature of 30 °C. All the measurements have been made using a du Nouy ring as the contact element. The data presented are equilibrium values where the surface tension values obtained between a set of three repeat measurements at a particular concentration agreed to within 0.5 of a $mN \cdot m^{-1}$. The samples were prepared in ultrahigh quality (UHQ) (18 MΩ) water in the same flask by means of 2-fold dilutions beginning at the highest concentration. Following dilution, each solution was temperature cycled by heating to above 60 °C and maintaining at 30 °C thereafter. The critical micelle concentration (CMC) is determined by plotting the variation in surface tension against log[concentration] and independently fitting the sub and supra CMC regions of the surface tension data to two linear equations. These are then equated to find their intersection on the log[*C*] ordinate. The antilog of this value gives the CMC, and the relatively large errors are a propagation of the minimum/maximum values on conversion from log[concentration].

2.4. Neutron Reflectivity. Neutron reflectivity measurements were made at the air−water interface on both the SURF and CRISP reflectometers at the ISIS pulsed neutron source, Chilton, Didcot, U.K.[19] During sample preparation, the samples were subjected to the same temperature cycling conditions as for the surface tension. All the measurements were carried out at a trough temperature of 30 °C (and in one case 45 °C). The measurements, which took around 20−30 min, were repeated over a time scale of 600 min to ensure that the surfaces had reached equilibrium.

The specular reflectivity is related to the Fourier transform of the scattering length density (or refractive index) distribution in a direction (z) normal to the surface or interface, such that

$$R(Q) = \frac{16\pi^2}{Q^2}\left|\int_{-\infty}^{\infty} \rho(z)\, e^{-iQz}\, dz\right|^2 \qquad (1)$$

where $\rho(z)$ is the scattering length density distribution, $\rho(z) = \sum_i N_i(z)\, b_i$, and N_i and b_i are the number density and scattering length, respectively, of species i. Q (or Q_z) is the scattering vector normal to the plane of the surface (the scattering vector, q, is defined as $Q = 4\pi \sin\theta/\lambda$, where θ is the glancing angle of incidence and λ is the neutron wavelength).[20] For a deuterium labeled surfactant in NRW, it has been shown[21] that the reflectivity arises only from the adsorbed surface layer. In the simplest case of a single monolayer, this can be analyzed as a layer of uniform composition to estimate

(12) McGillivray, D. J.; Thomas, R. K.; Rennie, A. R.; Penfold, J.; Sivia, D. S. *Langmuir* **2003**, *19*, 7719.
(13) Haas, S.; Hoffmann, H. *Prog. Colloid Polym. Sci.* **1996**, *101*, 131.
(14) Feitosa, E.; Cristina, P.; Barreleiro, A. *Prog. Colloid Polym. Sci.* **2004**, *128*, 163.
(15) Proverbio, Z. E.; Schulz, P. C.; Puig, J. E. *Colloid Polym. Sci.* **2002**, *280*, 1045.
(16) Soltero, J. F. A.; Bautista, F.; Pecina, E.; Puig, J. E.; Manero, O.; Proverbio, Z.; Schulz, P. C. *Colloid Polym. Sci.* **2000**, *278*, 37.
(17) Cocquyt, J.; Olsson, U.; Olfsson, G.; Van der Meeren, P. *Colloid Polym. Sci.* **2005**, *283*, 1376.
(18) www.kruss.info.
(19) http://www.isis.rl.ac.uk/LargeScale/SURF/surf.htm, http://www.isis.rl.ac.uk/LargeScale/CRISP/crisp.htm.
(20) Thomas, R. K.; Penfold, J. *J. Phys.: Condens. Matter* **1990**, *2*, 1369.
(21) Lu, J. R.; Thomas, R. K.; Penfold, J. *Adv. Colloid Interface Sci.* **2000**, *84*, 143.

the adsorbed amount. The reflectivity data were analyzed by fitting the reflectivity data to a model of a single adsorbed surfactant layer, a slab of uniform composition, which was found to be an adequate description of the adsorbed layer.[22] This provides a thickness, d, and scattering length density, ρ, from which the adsorbed amount of each surfactant can be obtained using

$$A = \frac{\Sigma b}{d\rho} \tag{2}$$

where A is the area per molecule of the surfactant. The surface excess follows from

$$\Gamma = \frac{1}{N_a A} \tag{3}$$

where N_a denotes Avogadro's number.

2.5. Small Angle Neutron Scattering (SANS). Small angle neutron scattering measurements were made using the LOQ diffractometer at the ISIS pulsed neutron source[23] and the D22 diffractometer at the Institut Laue Langevin (ILL).[24] For experiments performed at ISIS, data were recorded at a sample to detector distance of 4.5 m using the white beam time of flight method with 2−10 Å wavelength neutrons giving a Q-range of 0.008−0.3 Å^{-1}. A 12 mm diameter cadmium mask defined the illumination at the sample in 2 mm path length spectrophotometer cells. The SANS data were converted from time of flight to intensity versus scattering vector, and both were converted to absolute scale and radially averaged using standard procedures.[25] Data measured on D22 at the ILL were made using 8 Å wavelength neutrons at sample to detector distances of 17.6 and 3.5 m to give a combined Q-range of 0.002−0.2 Å^{-1}. The wavelength resolution was 10% $\Delta\lambda/\lambda$, and the collimation was set to 17.5 and 5.6 m, respectively. The sample mask in front of the 1 mm path length spectrophotometer cell was a slot 10 mm tall by 7 mm wide. The measured data were corrected for sample transmission and converted into an absolute scale using standard procedures.[26]

The general form of the scattering cross section variation with the scattering vector, Q, for discrete interacting and assuming spherically symmetric scattering with no polydispersity is given by

$$\frac{\partial\sigma}{\partial\Omega}(Q) = N\,P(Q)\,S(Q) + B_{\text{incoherent}} \tag{4}$$

where $P(Q)$ and $S(Q)$ are the aggregate form factor and interaggregate structure factor, respectively, and $B_{\text{incoherent}}$ is the sample dependent incoherent background. Two different models were used in the subsequent data analysis of the vesicular aggregates observed here. A core−shell model based on the Hayter−Penfold model[27−29] was used for the ultrasmall SANS (USANS) data and initially used for the SANS data. However, the 1-D lamellar "crystal" model based on the work of Nallet et al.[30] was predominantly used to characterize the scattering from the vesicles.

For a solution of globular polydisperse interacting particles (micelles, vesicles), the scattered intensity can be expressed in the decoupling approximation[27] as

$$\frac{d\sigma}{d\Omega}(Q) = N[S(Q)\,|\langle F(Q)\rangle_Q|^2 + \langle |F(Q)|^2\rangle_Q - |\langle F(Q)\rangle_Q|^2 \tag{5}$$

where the averages denoted by $\langle F(Q)\rangle_Q$ are averages over particles size and orientation, N is the particle number density, $S(Q)$ is the structure factor, and $F(Q)$ is the form factor. For a core and shell model[27] of the vesicles, the form factor can be written as

$$F(Q) = V_1(\rho_1 - \rho_2)\,F_0(QR_1) + V_2(\rho_2 - \rho_s)\,F_0(QR_2) \tag{6}$$

where $V_i = 4\pi R_i^3/3$ and $F_0(QR_i) = 3j_1(QR_i)/(QR_i) = 3[\sin(QR_i) - QR_i\cos(QR_i)]/(QR_i)^3$. ρ_1, ρ_2, and ρ_s are the scattering length densities of the micelle core, the micelle shell, and the solvent, respectively, and $j_1(QR_i)$ is a first order spherical Bessel function. The decoupling approximation assumes that there is no correlation between position and orientation and has been extensively used in the analysis of SANS data of a range of globular micelles and colloids.

Using the approach based on the work of Nallet et al.,[30] the vesicle lamellar phase scattering pattern can be analyzed to estimate the Caille constant (which is related to the bilayer rigidity, see below), the "d-spacing", and the number of layers/lamellar fragment. The analytical expression takes into account the lamellar form factor, $P(Q)$, and a structure factor, $S(Q)$, which accounts for the bilayer fluctuations, and assumes a powder average and a line shape width which includes the contribution from the instrumental resolution, such that

$$I(Q) = 2\pi\frac{V}{d}\frac{1}{Q^2}\,P(Q)\,\bar{S}(Q) \tag{7}$$

$$P(Q) = \frac{4}{Q^2}\Delta\rho^2\sin^2\left(Q\frac{\delta}{2}\right) \tag{8}$$

$$\bar{S}(Q) = 1 + 2\sum_1^{N-1}\left(1 - \frac{n}{N}\right)\cos\left(\frac{Qdn}{1 + 2\Delta Q^2 d^2\,\alpha(n)}\right)\times \exp\left\{-\frac{2Q^2d^2\,\alpha(n) + \Delta Q^2 d^2 n^2}{2(1 + 2\Delta Q^2 d^2\,\alpha(n))}\right\}\frac{1}{\sqrt{1 + 2\Delta Q^2 d^2\,\alpha(n)}} \tag{9}$$

where for small n

$$\langle (u_n - u_0)^2\rangle = \frac{\eta n^2 d^2}{8} \tag{10}$$

and $\alpha(n)$ is the correlation function

$$\alpha(n) = \langle (u_n - u_0)^2\rangle/2d^2 \tag{11}$$

N is the number of layers in a lamellar fragment, u_n is the displacement of the nth membrane along the z-direction, and η is the Caille parameter, which is related to the bilayer rigidity by

$$\eta = \frac{Q_0^2 k_B T}{8\pi\sqrt{K\mathrm{B}}} \tag{12}$$

where B and K are the bilayer compressibility and bending modulus of the bilayer array, respectively, ΔQ is the instrumental resolution, d is the lamellar d-spacing, δ is the bilayer width, $d = \delta/\phi$ (where ϕ is the volume fraction), and $Q_0 = 2\pi/d$. K is related to the single bilayer bending modulus, κ, where $\kappa = Kd$.

The resolution term σ_Q is calculated using[31]

$$\sigma_Q^2 = \left(\frac{Q}{\lambda}\right)^2\sigma_\lambda^2 + \left(\frac{Q}{\theta}\right)^2\sigma_\theta^2 \tag{13}$$

where the magnitude of the scattering vector at very small angles is defined by $Q = (4\pi/\lambda)\theta$, where 2θ is the scattering angle. The variance σ_λ^2 of the wavelength distribution is $(1/6)(\Delta\lambda)^2$, where $\Delta\lambda$ is the full-width half-maximum of the triangular function defined by the velocity selector. The dimensionless wavelength spread $\Delta\lambda/\lambda$ dominates at high Q. On the other hand, the variance σ_θ^2 of the scattering angle dominates at low Q. In order to account for these

(22) http://www.isis.rl.ac.uk/LargeScale/OpenGenie/OpenGenie.htm.
(23) Heenan, R. K.; King, S. M.; Penfold, J. *J. Appl. Crystallogr.* **1997**, *30*, 1140.
(24) Neutron Beam Facilities at the high flux reactor available for users, Institut Laue Langevin, Grenoble, France, 1994.
(25) Heenan, R. K.; King, S. M.; Osborn, R.; Stanley, H. B. RAL Internal Report, 1989, RAL-89-128.
(26) Ghosh, R. E.; Egelhaaf, S. U.; Rennie, A. R. Institut Laue Langevin Report, 1998.
(27) Hayter, J. B.; Penfold, J. *Colloid Polym. Sci.* **1983**, *261*, 1072.
(28) Hayter, J. B.; Hansen, J. P. *Mol. Phys.* **1982**, *42*, 651.
(29) Hayter, J. B.; Penfold, J. *Mol. Phys.* **1981**, *42*, 109.
(30) Nallet, F.; Laversanne, R.; Roux, D. *J. Phys. II* **1993**, *3*, 487.
(31) Grillo, I. ILL Technical Report, ILL01GR08T, 2001.

resolution effects in the Nallet model, the LOQ data were fitted using a mean wavelength of 6 Å, a $\sigma_\theta = 2 \times 10^{-3}$ rad. The $\Delta\lambda/\lambda$ contribution is negligible, and so σ_σ is dominated by the σ_θ term for the LOQ data. The D22 data were collected using 8 Å wavelength neutrons, 10% $\Delta\lambda/\lambda$, and $\sigma_\theta = 1 \times 10^{-3}$.[31]

2.6. Ultra Small Angle Neutron Scattering (USANS). USANS measurements, probing the Q-range 5×10^{-5}−5×10^{-3} Å^{-1}, were made using the BT5 beam line at the National Institute of Science and Technology, Gaithersburg, MD.[32] The lower Q limit corresponds to a dimension of 30 μm and overlaps well into the light scattering region. The upper limit overlaps the low Q limit of the D22 and D11 beam lines (0.6 μm). Obtaining data over these Q-ranges enabled sufficient overlap to allow the two data sets to be properly compared. Samples were prepared using 20 mm diameter quartz windowed cells with pathlengths of 2, 5, 7.5, and 10 mm depending on their scattering power. The selection of different pathlengths was to minimize the impact of multiple scattering. Data were corrected for slit smearing using an implementation of the Lake algorithm.[33] Analysis was performed by fitting the data to the core−shell model discussed in the previous section.

2.7. Photon Correlation Spectroscopy (PCS). The PCS measurements were made at Unilever Research, Port Sunlight, using a Malvern 4700 goniometer system, 7132 correlator, and version 1.41b of the software. The samples were used undiluted from their stock concentration of 1.5 mM, the light scattered at 90° was fluorescence filtered, and the photocathode was protected from overexposure by means of a 100 μm aperture.[34] A Lexel M85 argon ion laser was used as the light source, emitting 300 mW at a wavelength of 488.1 nm. Three measurements each of 120 s duration were made, and the autocorrelation functions were analyzed and fitted to a particle size distribution by means of the Contin program.[35] A Haake water bath was used to control the temperature at 30 °C.

2.8. Cryogenic Transmission Electron Microscopy (CryoTEM). TEM replication studies were made using a solution of DHDAB at a concentration of 10 mM (lower concentrations were attempted but the replicas were of poor quality) in order to support the SANS scattering data. The thermal instability and low surface tension of the sample provided some challenges to the freeze fracture replication (FFR) process, the result of which prevented the use of the slam freezing method. Successful replicas were achieved using an adapted process as follows: A small drop of the 10 mM solution was placed on a sheet of clean freshly cleaved mica clamped in the FFR sample holder while both were in an oven at 37 °C. This was immediately plunged into liquid nitrogen slush for 10 s and then transferred to liquid nitrogen. The FFR sample holder was then transferred into a Cressington CFE50 freeze fracture replication machine and allowed to etch at −85 °C for 5 min. The subsequent etched surface was coated with ∼2 nm of platinum/carbon at an angle of 45° followed by 8 nm of carbon normal to the surface. The sample was retrieved from the vacuum, and the surface replica floated onto water. Most of the replicas were captured onto 200 mesh copper TEM grids. The replicas were examined in a Philips CM120 transmission electron microscope at 120 kV. Various images from the replicas were recorded at a magnification of 20 000 times.

3. Results and Discussion

3.1. Surface Tension and Kinetics of Absorption. The optimum means for suitably preparing DHDAB solutions for measurement of surface tension was determined by extensive systematic studies as described earlier. The surface tension was measured every 5 min until the solution had come to equilibrium. Figure 1 shows the variation in surface tension with time at concentrations of 1×10^{-4}, 5×10^{-5}, and 2.5×10^{-5} M. For all the solutions studied, surface equilibrium (where the surface

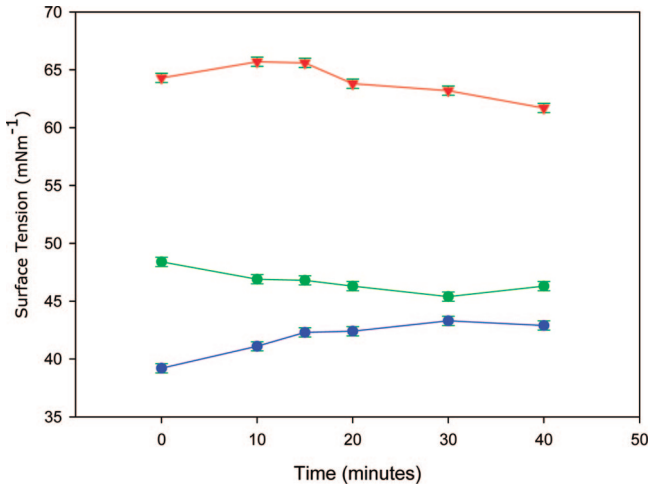

Figure 1. Kinetics of surface equilibrium in pure DHDAB at concentrations of 1×10^{-4} (blue), 5×10^{-5} (green), and 2.5×10^{-5} (red) M.

settles to a consistent surface tension) is reached after 15−20 min and is independent of solution concentration.

Conventional surface tension measurements exhibit time effects at very low solution concentrations and when impurities are present. The concentration dependence indicates that impurities are extremely unlikely here, and the drift with time does not follow the normal pattern associated with the presence of impurities. Here, the slow kinetics are attributed to slow kinetics of dissolution of the bulk aggregates. Each pull of the ring through the surface disturbs and depletes the surface, and monomer immediately adjacent to the interface diffuses into the surface region to restore the equilibrium surface pressure. Monomer able to reach the surface within the diffusion length (a few micrometers) diffuses to the surface in order to compensate for the surface depletion, but, because of the low solution monomer activity, the local reservoir is unable to compensate for the local depletion in monomer concentration in this near surface region, thereby creating a temporary depletion layer. The extent to which this region is depleted of surfactant monomer is always constant due to the ring area. However, the ability of the solution to recover depends on the ambient surfactant monomer activity. As this rises, the solution becomes better able to reach a reproducible surface pressure, and as the interval between repeat measurements was always 5 min, a reproducible state (if not equilibrium) is achieved once the ambient solution monomer concentration has reached a sufficiently high level.

Having established the time scales for the surface to achieve equilibrium, the variation in surface tension with solution concentration of DHDAB was determined. Beginning at the highest concentration, the surface tension of each solution was measured. The next concentration was prepared by diluting the remainder of the solution by a factor of 2, which was heated to 60 °C for 20 min and allowed to cool to 30 °C prior to measurement. The variation in surface tension with concentration obtained in this way is shown in Figure 2.

Analysis of the data presented in Figure 2 (using the process described previously in section 2.3) produced a value for the DHDAB CAC of $5 \pm 3 \times 10^{-5}$ M. This is considerably higher than those which had been previously reported in the literature[6,13,17] but is in good agreement with an extrapolation based on the work of Bai et al.[36] using DSC. From the gradient of the

(32) Barker, J. G.; Glinka, C. J.; Moyer, J. J.; Kim, M H.; Drews, A. R.; Agamalian, M. *J. Appl. Crystallogr.* **2005**, *38*, 1004.
(33) Lake, J. A. *Acta Crystallogr.* **1967**, *23*, 191.
(34) (a) American National Standards Institute, 1996, ISO:13321. (b) Horne, D. S. *J. Phys. D: Appl. Phys.* **1989**, *22*, 1257.
(35) Provencher, S. W. *Makromol. Chem.* **1979**, *180*, 201.
(36) Bai, G.; Wang, J.; Yan, H.; Li, Z.; Thomas, R. K. *J. Phys. Chem. B* **2001**, *105*, 9576.

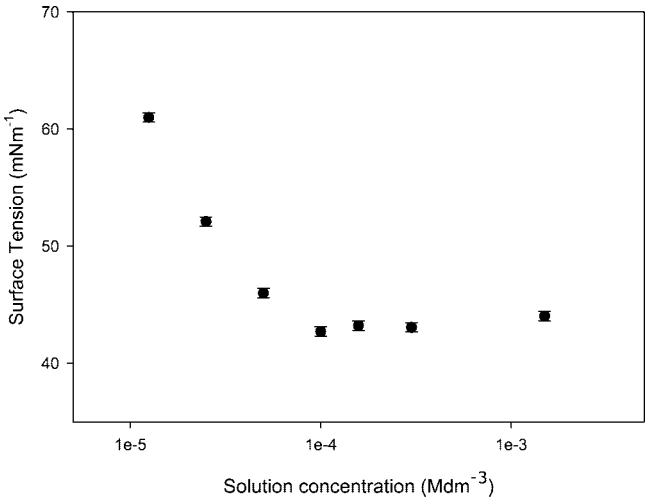

Figure 2. Variation in DHDAB surface tension with concentration.

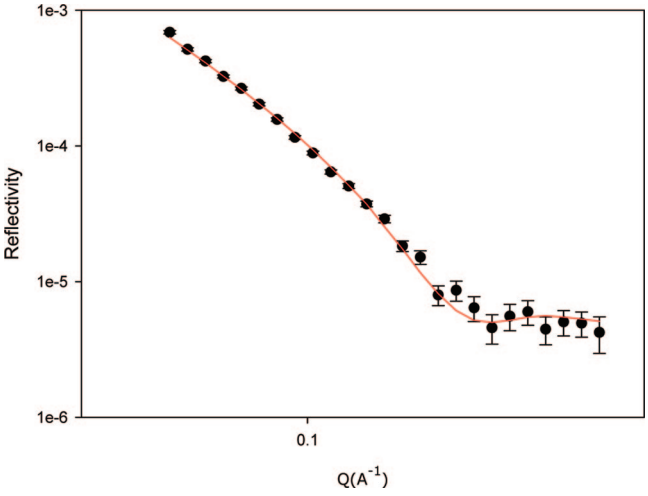

Figure 3. Neutron reflectivity curve ($R(Q)$ vs Q) for 3×10^{-4} M *d*-DHDAB in null reflecting water at 30 °C after 3.5 h. The data are the points, and the red line is the output from a fit to the single layer model. The background is included as part of the fitting process.

sub-CAC region, $d\gamma/dc_1$, measured as 6.75×10^{-4} N m^{2-} mol^{-1}, the limiting surface excess and area per molecule were calculated from the Gibbs equation. The DHDAB limiting surface excess is $2.6 \pm 0.1 \times 10^{-10}$ mol·cm^{-2}, and this is equivalent to an area per molecule of 62 ± 1 Å^2. This limiting area per molecule is close to predictions for dialkyl chains by Tanford,[37] to values recently reported for dichain alkylbenzene sulfonates by Ma et al.,[38] and to that previously reported for DHDAB.[39]

3.2. Neutron Reflectivity Studies. The neutron reflectivity data shown in Figure 3 for 3×10^{-4} M *d*-DHDAB in NRW are typical of the data which were measured and represent equilibrium data. The line is the fit to the data obtained using the uniform thickness slab model described earlier in the Experimental Details section.

From the fit of the data as a single uniform layer (see earlier), the layer thickness, scattering length density, and hence surfactant area per molecule and surface excess, as listed in Table 1, are obtained. The DHDAB area per molecule and limiting surface

Table 1. Summary of Data Obtained from Single Uniform Slab Fit to Reflectivity Curve for 3×10^{-4}M *d*-DHDAB in NRW at 30 °C[a]

D (Å)	23 ± 1
ρ ($\times 10^{-6}$ Å^2)	4.6 ± 0.05
A (Å^2)	62 ± 1
Γ ($\times 10^{-10}$ mol·cm^{-2})	2.7 ± 0.1

[a] Note: The Σb for *d*-DHDAB is 6.60×10^{-3} Å.

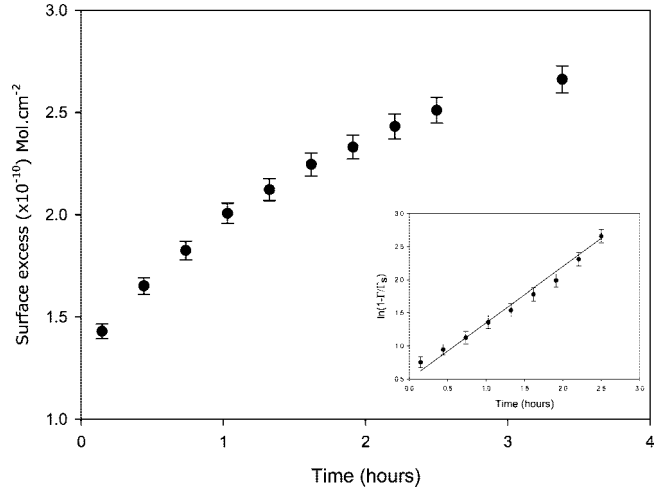

Figure 4. Evolution of the surface excess with time for a solution of 3×10^{-4} M *d*-DHDAB in null reflecting water at 30 °C. The inset is a fit to the kinetics of adsorption.

excess derived from neutron reflectivity are in excellent agreement with those derived from surface tension.

The neutron reflectivity measurements typically require a minimum time of 20 min in order to obtain data of a sufficient standard. Hence, the ability to observe kinetic processes is therefore limited to those which require at least double this period in order to attain equilibrium. The evolution of the adsorbed layer with time was studied for a range of solution concentrations, and there were only slight differences in kinetics between the data obtained for both high and low surfactant concentrations. Figure 4 shows an example of the variation in surface excess with time obtained at a concentration of 3×10^{-4} M.

The data in Figure 4 show that the surface evolves with time and that the kinetics of adsorption are rather slow, requiring over 3 h to reach the limiting surface excess obtained from surface tension. This would imply that different kinetics of adsorption are being observed for the two methods. However, this is associated with differences in the measurement methods. The key differences between the neutron reflectivity (NR) and the surface tension measurements are that in surface tension measurements the surface is continually disturbed, whereas in neutron reflection the interface is left to achieve equilibrium without perturbation. Furthermore, the geometry of the sample reservoirs are very different. The trough used in reflectivity presents a large flat surface to the neutron beam, and this is achieved by having a long thin flat strip of fluid as the sample, and in contrast the Kruss dish for the surface tension measurements is narrow and deep. Thus, convection can play a much greater role in distributing dissolved surfactant monomer in the surface tension measurements, whereas diffusion processes are the dominant monomer transport in neutron reflection sample geometry.

The variation in equilibrium surface excess with concentration, as determined via neutron reflectivity, for DHDAB is shown in Figure 5, from which the limiting surface excess and CAC were

(37) Tanford, C. *The Hydrophobic Effect*; Wiley: New York, 1973.
(38) Ma, J.-G.; Boyd, B. J.; Drummond, C. J. *Langmuir* **2006**, *22*, 8646.
(39) Penfold, J.; De Sivia, D. S.; Staples, E.; Tucker, I.; Thomas, R. K. *Langmuir* **2004**, *20*, 2265.

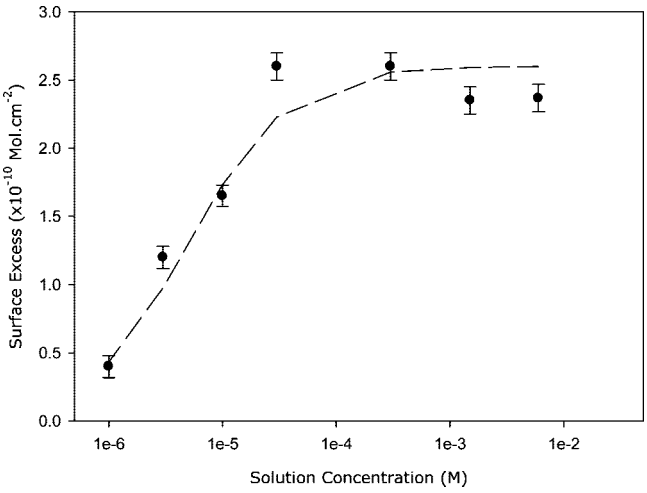

Figure 5. Surface excess varation with concentration for *d*-DHDAB in null reflecting water at 30 °C. The dashed line is a fit to the data using a Langmuir isotherm.

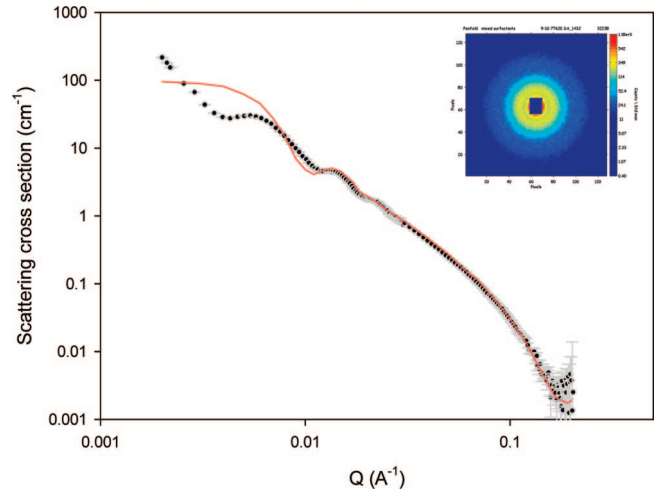

Figure 6. Scattering from 1.5 mM DHDAB in D_2O at 30 °C. The red line is the fit to a polydisperse core−shell model.

obtained. The limiting surface excess is $2.6 \pm 0.2 \times 10^{-10}$ mol·cm^{-2}, in very good agreement with that obtained from the sub-CAC region of the surface tension data. The CAC was determined as $3 \pm 1 \times 10^{-5}$ M. The values obtained using the two techniques are in reasonable agreement with each other. However, the CAC values determined in the current study are considerably higher than those reported by Haas et al.[6,13] and predicted by Nagarajan.[40] Condensed phases in the related system, di-C_{18}DAB, deposited at the air−water interface by Langmuir−Blodgett film methods have been reported by Taylor et al.[41] The corresponding area/molecule of 58 Å^2 is also in reasonable agreement with that obtained for di-C_{16}DAB in the current study.

Equivalent neutron reflection measurements at 45 °C (where the DHDAB is now in the fluidic L_α phase) provided a CAC of $\sim 8 \pm 0.5 \times 10^{-6}$ M, and with faster kinetics of adsorption. That the CAC in the L_α phase is different by 1 order of magnitude from that in the L_β phase reflects the greater ease of self-aggregation in the L_α phase.

The variation of the equilibrium DHDAB adsorption with surfactant concentration is well represented by a Langmuir isotherm of the form

$$\Gamma = \Gamma_s c \Big/ \left(c + \frac{1}{k}\right) \tag{14}$$

where Γ is the adsorbed amount, Γ_s is adsorption at saturation (or limiting surface excess), c is the surfactant concentration, and k is the equilibrium adsorption coefficient. The dashed line in Figure 5 is a fit to eq 14 for $\Gamma_s = 2.6 \pm 0.2 \times 10^{-10}$ mol·cm^{-2} and $k = 2 \times 10^5$ L·mol^{-1}.

Assuming that the kinetics of adsorption can also be described by the simple Langmuir approach, then the time dependence of the adsorption is of the form

$$\left(1 - \frac{\Gamma}{\Gamma_s}\right) = \exp\left(-\frac{t}{\tau}\right) \tag{15}$$

where τ is now the characteristic time for equilibrium adsorption. A plot of $\ln(1 - \Gamma/\Gamma_s)$ versus time is approximately linear, as shown in the inset in Figure 4, and provides a characteristic time scale for adsorption of approximately 50 min.

3.3. Solution Behavior of Pure DHDAB. *3.3.1. SANS Studies of Pure DHDAB.* Figure 6 shows the SANS scattering for 1.5 mM h-DHDAB in D_2O. The inset in Figure 6 shows that the 2-D scattering pattern in dilute DHDAB is isotropic. The 2-D scattering remains essentially isotropic for concentrations up to 400 mM (~20 wt %), the highest concentration measured. This means that the scattering is either due to spherically symmetric objects or from fragments which are sufficiently small that they are isotropically oriented within the solution. A more detailed analysis of the radially averaged data indicate that this is not entirely the case.

An initial qualitative inspection suggests that the data are consistent with the scattering from relatively monodisperse spheres. Such an approach has provided acceptable model fits to other vesicle data reported in the literature.[42,43] However, attempts to model the current data using such an approach resulted in unacceptably poor fits. An example of the misfit which is obtained using the core−shell model is shown by the red line in Figure 6. It is possible to match some of the oscillations (the visibility of the oscillations is consistent with low polydispersity) but not all of them, and clearly the core−shell form factor is not appropriate. Furthermore, large values of polydispersity are required to match the degree of damping of the oscillations (>50%). Superficially similar SANS data from vesicles composed of sodium dodecyl benzenesulfonate/imidazoline/water mixtures reported by Gonzalez et al.[43] were fitted to a polydisperse core−shell model, with polydispersity values in the range 0.24−0.6, depending on the actual system. However, the more limited Q-range of that data rendered only one oscillation clearly visible in the scattering data, compared to approximately three clear oscillations for the system studied herein. Furthermore, in order to match the scattering, particularly at high Q, an unacceptably low value of the bilayer thickness has to be used. The oscillations have the correct interrelationship expected for a lamellar phase, particularly evident when the data were replotted as IQ^2 versus Q. In Figure 7, the same data presented in Figure 6 are displayed as IQ^2 versus Q, with the corresponding fit to the Nallet lamellar model.

As can be seen in Figure 7, the 1.5 mM DHDAB SANS data are well fitted by the Nallet model. Similar data and fits were obtained for solution concentrations up to and including 80 mM, and for this concentration range the number of layers was

(40) Nagarajan, R. *Chem. Eng. Commun.* **1987**, *55*, 261.
(41) Taylor, D. M.; Dong, Y.; Jones, C. C. *Thin Solid Films* **1996**, *284-285*, 130.
(42) Neih, M.-P.; Raghunathan, V. A.; Kline, S. R.; Harroun, T. A.; Huang, C.-Y.; Pencer, J.; Katsaras, J. *Langmuir* **2005**, *21*, 6656.
(43) Gonzalez, Y. I.; Stjerndahl, M.; Danino, D.; Kaler, E. W. *Langmuir* **2004**, *20*, 7053.

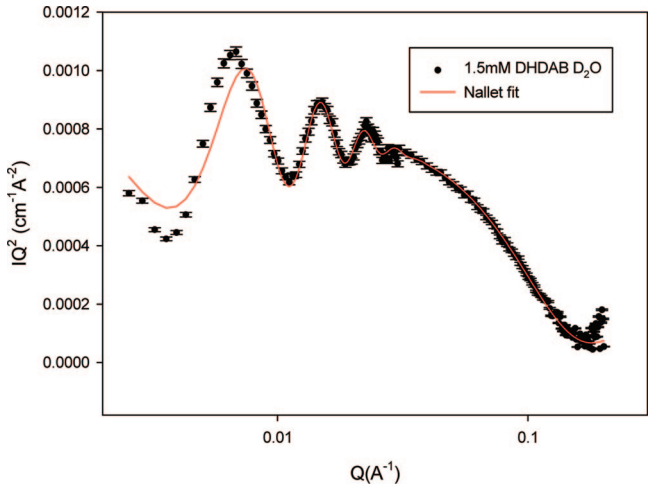

Figure 7. Scattering from 1.5 mM DHDAB in D_2O at 30° displayed as IQ^2 versus Q to amplify the lamellar phase. The red line is a fit to the data using the Nallet lamellar phase model.

Table 2. Fits to the Nallet Model for DHDAB Dispersions in D_2O at 30 °C

concentration (mM)	layer spacing, d (Å) (±5)	layer thickness, δ (Å) (±0.2)	Caille parameter, η (±0.01)	no. of layers, N	phase volume, ϕ
1.5	850	33.7	0.07	2	0.0007
10	785	33.4	0.07	2	0.006
20	550	34.0	0.07	2	0.019
30	505	33.9	0.07	2	0.024
40 (LOQ)	450	33.9	0.07	2	0.028
40 (ILL)	380	33.6	0.12	2	0.029
60	400	33.5	0.15	2	0.037
80 (LOQ)	370	33.2	0.20	2	0.049
80 (ILL)	330	33.7	0.20	2	0.051

consistent at $N = 2$. Above 80 mM, the model fits to the data were less good. In Figure 7, there is a slight mismatch between the model and the data in the low Q region of the scattering, and this is typical of the data that has been analyzed quantitatively at other concentrations. This region of the data/model is particularly sensitive to the instrument resolution, which is varying significantly in this region, and the discrepancy is attributed to the deficiencies in the exact form of the resolution function. Some modest differences in the fitted model parameters (most notably the d-spacing) obtained for data measured at ISIS and at the ILL for what is nominally the same system are evident in Table 2. These were not physically the same samples and in part reflect the reproducibility of the samples in the bulk. However, the form of the resolution is different for the two instruments and is much worse for LOQ in the low Q region where the d-spacing of the vesicles is predominately determined. Hence, the differences in part reflect the greater uncertainty associated with extracting the model parameters for the LOQ data due to inferior resolution. Throughout this concentration range, the bulk aggregates are best described as bilamellar vesicles, that is, spherical aggregates bounded by two rings of surfactant bilayers themselves separated by a layer of solvent. Figure 8 shows a schematic of both bilamellar (BLV) and multilamellar vesicles (MLV).

The results of data analyzed using the Nallet model for DHDAB concentrations between 1.5 and 80 mM DHDAB in D_2O are summarized in Table 2. In some cases, duplicate data sets were collected on the D22 diffractometer and the model fits to both sets of data are included for completeness.

In the concentration range 1.5−80 mM, the scattering data are consistent with bilamellar vesicles as described above and appear to be single phase. At the lowest concentrations measured, there is no evidence for a competing micellar phase or for a purely micellar region. Hence, the onset of aggregation (as observed by NR and ST) is described as a CAC and not a critical micelle concentration, CMC. For concentrations in excess of 80 mM, the scattering, although still isotropic, is more complex (not shown here) and the solution is not a single phase. The scattering is now consistent with coexistent BLV and L_β lamellar phase components, but this is now too complex to provide any quantitative analysis.

The bilamellar vesicle model provides an excellent description of the data and, as expected, the interlayer spacing decreases with increasing surfactant concentration. The phase volumes in Table 2, derived from the absolute scaling of the data, are lower than would be expected from calculations but are still in reasonable agreement (Supporting Information, section 1) with a simple model of the bilamellar vesicle. What is unusual, however, and characteristic of the model is that the interlayer spacings (and consequently d-spacings) are exceptionally large. The thickness of the bilayer remains essentially constant and is consistent with an interdigitated conformation of a bilayer of DHDAB molecules. Increasing the number of layers in the model at these lower surfactant concentrations in general resulted in worse fits to the data. The variation of the d-spacing with the vesicle phase volumes obtained from the data analysis is shown in Figure 9. For a continuously swelling lamellar phase, a plot of d-spacing against $1/\phi$ (where ϕ is the phase volume) (inset in Figure 9) should be linear with a slope that is related to the hydrocarbon layer thickness, δ, by the relationship $d_o = \delta/\phi$. Although the relationship is linear, this analysis gives a very low value of δ that is approximately 6 Å, which is physically unrealistic. This is further evidence that this system does not exist in the form of a classical continuous lamellar phase and, by inference, corroborates the BLV format of the lamellae.

For the concentration range 1.5−80 mM the BLV model is a good representation of the experimental data. It should be noted that data collected at high solution concentrations did not fit the bilayer vesicle model as well and that, at concentrations of 200 mM and higher, additional unattributed contributions to the radially averaged scattering at low angle are evident. Hence, quantitative analysis at these higher concentrations was not performed.

To support and/or confirm the interpretation of the SANS data in terms of the BLV model, other complementary techniques were used, (USANS, DLS, and CryoTEM). Particle sizing is perhaps the next simplest method, and, using the data in Table 2, an estimate of the particle diameter can be derived.

USANS data obtained using the BT5 instrument at NIST were analyzed in two different ways. A Guinier analysis of the slit smeared raw USANS data for 1.5 mM h-DHDAB in D_2O gave a radius of gyration, R_g, of 1050 Å, corresponding to a particle radius of 1360 ± 140 Å, assuming a solid sphere (where $R = \sqrt{(3/5)}R_g$), or for a hollow sphere with a thin shell, where $R = R_g$, a radius of 1050 Å. For the bilamellar structure, $R = R_g$ is probably more correct, but for the MLV structure $R = \sqrt{(3/5)}R_g$ is probably closer. As the analysis is only approximate, the 20% difference between the two is not significant, and what is more important is that the predicted R_g values are in close agreement with the dimension predicted by the calculations based on bilamellar vesicles and the Nallet analysis at higher Q for this concentration. The desmeared data were also simulated using the original core−shell polydisperse vesicle model (see Figure 1 in the Supporting Information), where the shell of the liposome is constrained using the previously determined parameters. The

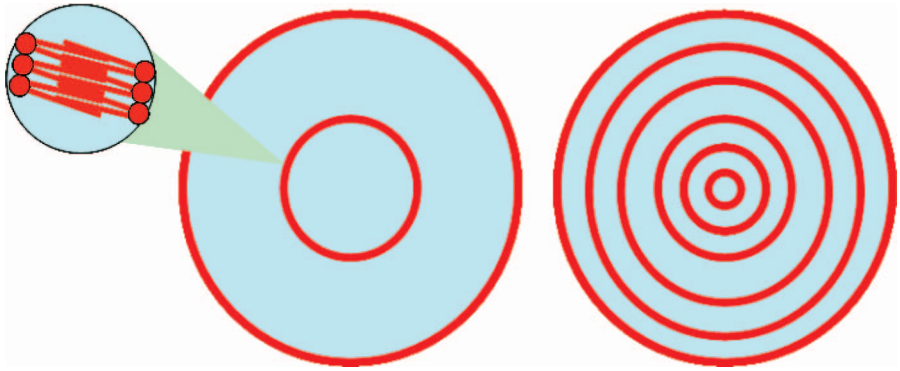

Figure 8. Schematic of (a) bilamellar vesicle and (b) multilamellar vesicle ($N = 6$). The blue denotes solvent, and the red denotes a surfactant bilayer region.

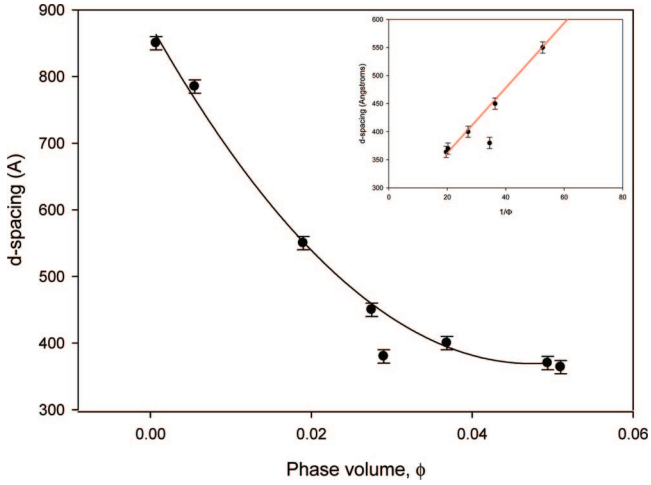

Figure 9. Variation in lamellar d_o spacing with vesicle phase volume. The inset is the prediction of the continuously swelling lamellar phase model.

result is a core diameter of 2750 Å and polydispersity of 1350 Å. Both analyses are highly consistent with the particle dimension predicted using the results from the Nallet model which predicts a vesicle radius of 1320 Å, and hence, the USANS results support the BLV interpretation.

3.3.2. CryoTEM Imaging. The replicas were examined in a Philips CM120 transmission electron microscope at 120 kV, and examples of images recorded are shown in Figure 10 at a magnification of 20 000 times.

There are still typical electron microscopy artifacts present in these samples, but there are also ringed structures consistent with vesicles of some 200−300 nm diameter. The ultimate aim of this work was to corroborate the DHDAB microstructure model. Although the electron microscopy images are not optimal, they do contain evidence which supports the chosen model, that is, lamellar coated vesicles. However, it is clear that this approach cannot be used reliably on these particular systems.

3.3.3. Sizing by PCS. PCS measurements on the undiluted samples at 30 °C gave autocorrelation functions typical of particles in the range 100−500 nm, and the results of analyses showed a high degree of experimental reproducibility (section 2 (Table 1) in the Supporting Information). The mean particle radius of the 1.5 mM DHDAB in D_2O was 1115 ± 42 Å with a polydispersity of 65%. These dimensions are also in close agreement with the predictions of the BLV model and in reasonable agreement with the USANS (particularly the polydispersity) data. The latter further serves to confirm the BLV structure, as polydispersity of this magnitude would tend to smear out the observed intensity modulations (which are in fact Bragg modulations) as seen in Figures 6 and 7. In contrast, Bragg scattering from lamellar ordering would be largely unaffected unless the polydispersity was coupled with a change in the bilayer rigidity.

4. Discussion

At the outset, there were concerns regarding whether the system had actually reached equilibrium. The most sensitive probe of the monomer activity is the surface activity, and the sample preparation process was refined during initial surface tension studies until the same response (as shown in Figure 4) was obtained for repeat measurements at the same solution concentration. Various attempts were made to force the system into a different thermodynamic state, and only when the preheat temperature was close to the L_α/L_β transition temperature were any variations noted. Thus, if these solutions are not at true thermodynamic equilibrium, then at least they are at a reproducible nonequilibrium. The relative proximity to the Krafft point did not seem to be an important factor, provided the solutions were not allowed to cool to below 30 °C having been preheated to 60 °C and then cooled to 30 °C. Solutions prepared in this way and placed on long-term storage at this temperature were colloidally stable for ∼24 months.

A significant observation from this study is that DHDAB is more soluble than previously reported. The CAC for DHDAB is approximately 1 order of magnitude larger than expected on the basis of other reported studies[6,13,39] and the predictions of molecular modeling.[40] The agreement between the experimentally determined CAC values, $5 \pm 3 \times 10^{-5}$ M from surface tension and $3 \pm 1 \times 10^{-5}$ M derived using neutron reflectivity, is relatively good. Furthermore, the fact that the surfactants used in the two different measurements are two entirely independent versions of the same material gives additional confidence to these new values for the DHDAB CAC.

The neutron reflectivity data for the adsorption of DHDAB are consistent with a monolayer adsorbed at the air−water interface, with a thickness of around 23 Å and an area/molecule of ∼60 Å^2 at the CAC (at 30 °C), similar to that previously observed by Penfold et al.[39] In the presence of electrolyte and at elevated temperature (>40 °C), Penfold et al.[39] observed more complex surface behavior and the formation of multilayer structures at the interface. In their pioneering work on phospholipids, Gershfeld et al.[44,45] observed within a narrow temperature range above the gel−crystalline transition temper-

(44) Gershfeld, N. L.; Stevens, W. F.; Nossal, R. J. *Faraday Discuss. Chem. Soc.* **1986**, *81*, 19.
(45) Gershfeld, N. L. *Biophys. J.* **1986**, *50*, 457.

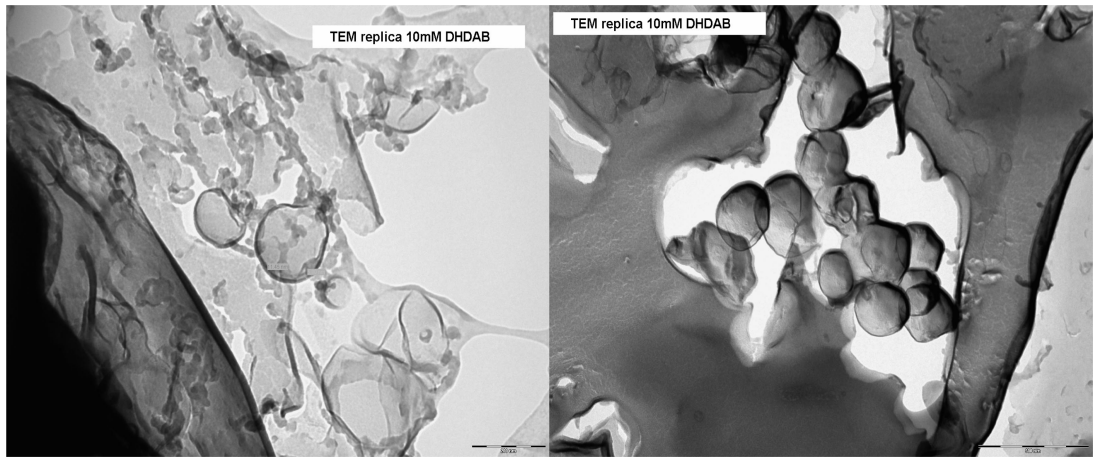

Figure 10. Replica CryoTEM images of 10 mM DHDAB in water. Magnification is ×20 000.

ature that bilayer formation at the air−water interface occurs, associated with vesicle adsorption. There is no evidence in the data presented here for any form of adsorption other than a monolayer of DHDAB.

The neutron reflectivity measurements have shown that the surface takes approximately 3−4 h in order to fully reach equilibrium. The relatively high CAC is not consistent with the initial hypothesis that slow kinetics are a direct consequence of vanishingly small monomer concentrations due to a low CAC.[41] Instead, it is postulated here that the slow dynamics are a consequence of a low near surface monomer concentration associated with a slow rate of dissolution from the aggregates. This concept was briefly discussed previously in the context of the surface tension measurements. The apparent differences in the kinetics derived from neutron reflection and surface tension measurements can be explained by the different methodologies. The act of pulling the ring through the surface disturbs the surface and contributes to bulk transport of monomer throughout the volume of liquid in the disk. However, in neutron reflectivity experiments, the surface is undisturbed and the surface equilibration times are significantly longer. The consequence of having a thin layer of liquid in the trough is that convection cannot play any part in transporting fresh monomer to the interface. The adsorption process is purely diffusive and limited by the solution monomer activity. The conundrum is that the CAC is relatively high and yet the air−water interface adsorbed layer requires approximately 3−4 h to reach equilibrium. Unlike the case of conventional surfactant aggregates, there is a large barrier to monomer dissolution from the bulk aggregate. If the monomer lifetime in the vesicle is sufficiently long that the only significant source of monomer for the surface is that which is already in solution at the CAC, then the problem becomes a one-dimensional diffusion limited transport to the surface in the height direction only. The time scale for monomer diffusion to transport sufficient DHDAB to the interface so as to achieve the equilibrium surface excess has been calculated as between 7 and 22 min, considerably shorter than the actual time required, indicating that slow dissolution from the aggregates is responsible for the long equilibration times. Although not conclusive, this is sufficient to support the slow dissolution hypothesis, and further work on determining the bulk aggregate lifetime is planned.

There are several comprehensive reviews concerning kinetics of surface adsorption,[46–50] and all of these focus on the situation where the surfactant has a relatively high CAC and has fast kinetics of micelle dissolution, and where the surface is being strained in some way, for example, under flow conditions as could be experienced in dynamic surface tension measurements. Breward and Howell[46] predict regions in straining flow where the subsurface solution structure contains a region immediately adjacent to the interface which contains no micelles, and in which the monomer concentration is in fact lower than the bulk. Noskov[50] describes the reliance of dynamic surface tension on the relative rate of dissolution of bulk aggregates (micelles). All of these studies however refer to dynamic surface conditions, whereas the work presented here is under equilibrium conditions. An opportunity for further work therefore exists where the limiting factors are a low CAC and a very slow aggregate disintegration rate. Cocquyt et al. observed a slow transition using DSC in di-C_{18}DAB but did not interpret the data quantitatively.[17] Taylor et al. also observed slow kinetics of adsorption in di-C_{18}DAB but did not report the time scale for the surface to reach equilibrium.[41]

In solution, the bulk aggregates exist as bilamellar vesicles of approximately 1300 Å radius. The solution microstructure of DHDAB is comparable to that reported for the di-C_{12}DAB variant by Proverbio et al.[15] and Soltero et al.[16] Neih et al.[42] have reported the formation of unilamellar vesicles under similar preparation conditions in dimyristoyl phosphatidylcholine and related systems, whose lamellar *d*-spacings are similar to those reported here. Cocquyt and co-workers reported particle sizes in the related system di-C_{18}DAB of the order of 1200−1500 Å at temperatures comparable with those in the current study.[17] Optical and transmission electron microscopy studies by Kopade et al.[51] in anionic phospholipids again show spherical objects of the order of 1000 Å. Feitosa et al. have recently reported similar sizes using PCS for di-C_{12}DAB.[52] Radlinska et al.[11] have reported a more complex phase behavior than is observed here in the related system didodecyl dimethylammoniumacetate, the di-C_{12} variant with the counterion replaced by acetate. At low phase volumes, they report a thermodynamically stable vesicular phase. For phase volumes exceeding 0.0005, a more complex solution behavior (a symmetric sponge phase coexisting with a lamellar phase) is reported. Other evidence for the existence of bilamellar vesicles

(46) Breward, C. J. W.; Howell, P. D. *Eur. J. Appl. Math.* **2004**, *15*, 511.
(47) Dushkin, C. D. *Colloids Surf., A* **1998**, *143*, 283.
(48) Danov, K. D.; Vlahovska, P. M.; Horozov, T.; Dushkin, C. D.; Kralchevsky, P.; Mehreteab, A.; Broze, G. *J. Colloid Interface Sci.* **1996**, *183*, 223.
(49) Chang, C.-H.; Franses, E. I. *Colloids Surf., A* **1995**, *100*, 1.
(50) Noskov, B. A. *Adv. Colloid Interface Sci.* **2002**, *95*, 237.
(51) Khopade, A.; Shenoy, D. B.; Khopade, S. A.; Jain, N. K. *Langmuir* **2004**, *20*, 7368.
(52) Feitosa, E.; Jansson, J.; Lindman, B. *Chem. Phys. Lipids* **2006**, *142*, 128.

or vesicles with a small number of bilayers have been reported by Gonzalez et al.[43] for sodium dodecyl benzenesulfonate/imidazoline/water mixtures and Douliez et al.[53] for the ethanolamine salt of 12-hydroxysearic acid in water. Hence, there is considerable evidence for the formation of such BLV structures in related systems in the current literature. No evidence has been found to support more complex solution behavior other than lamellar vesicles over the concentration range 1−80 mM in the di-C_{16}DAB system as discussed earlier. The higher concentration solution microstructure is more complex and will form the basis of further study. Up to a concentration of 80 mM, the solution is a single phase and the microstructure is well described as bilamellar vesicles (see Table 2). Above 80 mM, the Nallet analysis no longer provides an adequate description of the data, and it is consistent with the coexistence of bilamellar vesicles and an L_β lamellar phase. Hence, any detailed quantitative evolution of this higher concentration region is not possible.

Different theoretical approaches have been applied to the formation of vesicles in solution. The thermodynamics of lamellar fragment formation compared to vesicle formation has been considered by Bryskhe et al.,[54] and this will be considered below in the context of the data reported here. Jung et al.[55] have considered the origins of stability in spontaneous vesicle formation by comparing the contributions of undulations and spontaneous curvature. Where the bending modulus, κ, is $\sim k_BT$, equilibrium unilamellar vesicles are stabilized by undulation forces. However, where $\kappa \gg k_BT$, unilamellar vesicles are stabilized by the spontaeous curvature, and a narrow distribution of vesicle radii are favored. Measured size distributions for unilamellar vesicles from the mixtures of cetyltrimethylammonium bromide (CTAB) and sodium octyl sulfonate (SOS), and CTAB/sodium perfluorooctanoate (SPO) mixtures were consistent with those arguments. Furthermore, the addition of electrolyte to CTAB/SPO mixtures was sufficient to change the spontaneous curvature to favor formation of bilamellar vesicles. It was not possible to get reliable estimates of the size distribution for DHDAB from CryoTEM images or from the light scattering data, although the estimates for the USANS data were broadly consistent with the values reported by Gonzalez et al.[43] Fogden et al.[56] have discussed in more detail the theoretical treatment of surfactant membrane bending energy and the role of spontaneous curvature.

Bryskhe et al. have discussed the relative stability of vesicles and lamellar fragments by considering the thermodynamics of the two solution microstructures.[54] They describe the relative stability of discotics and vesicles as arising from a difference between the vesicle curvature energy and the disk edge line energy. The difference in excess free energy between vesicle and disk, ΔG, can be calculated using

$$\frac{\Delta G}{\kappa'} = 8\pi(1 - \alpha_s) \tag{16}$$

where κ' is the bilayer rigidity, equivalent to κ in eq 18, and α_s is a stability parameter related to the line tension λ_m and the bilayer area a_B,

$$\alpha_s = \frac{\lambda_m\sqrt{a_B}}{4\kappa'\sqrt{\pi}} \tag{17}$$

α_s predicts the preference of the system to form discs ($\alpha_s < 1$) or vesicles ($\alpha_s > 1$). Using eqs 16 and 17, both α_s and the disk/vesicle free energy difference have been calculated, and some relevant examples are summarized in Table 2 in the Supporting Information. For realistic estimates of parameters derived from this and other studies,[4,53] vesicle formation becomes thermodynamically favored for radii between 1000 and 1500 Å. Reducing the bilayer rigidity by 40% will favor small vesicles, and a 10-fold reduction in the surfactant bending modulus ($3-5k_BT$) is required in order to stabilize discotic structures. Experimentally, the lamellar *d*-spacing decreases from 890 to 385 Å as the solution concentration increases from 1.5 to 80 mM, but the Caille parameter changes from 0.07 to 0.2. In order to make comparisons with the predictions of Bryskhe et al., the results of the Nallet type analysis can be converted into an equivalent parameter, that is, the product of the single bilayer bending modulus, κ, and bilayer compressibility, B. From the definition of the Caille parameter in eq 12, the product of B and κ can be determined by rearranging eq 12 and casting it in terms of the lamellar *d*-spacing such that

$$\sqrt{\frac{\kappa B}{d_o}} = \frac{\pi k_B T}{2d_o^2\eta} \tag{18}$$

The separation of the compressibility and bending moduli have been determined by performing systematic studies of continuously swelling systems, as demonstrated in several different systems,[10,58] using the "excess area method". However, for DHDAB, the swelling region is confined to a narrow range of phase volumes over which the vesicle lamellar *d*-spacing varies with phase volume, but, given the inability to predict the bilayer thickness, the data in the swelling region are not compatible with the excess area approach. Hence, for the DHDAB system, this separation is not possible and the analysis provides only the product of κB. However, given that the bilayer spacing varies only by a factor of 2 over this concentration range (factor 50), the initial assumption made was that the bilayer compressibility is essentially constant, and therefore any changes in the product of κB are predominantly due to changes in membrane rigidity, κ. From calculations based on the work of Bryskhe et al.[55] (Supporting Information, section 4, Table 2a−c), a 10-fold decrease in κ is necessary to transform the solution microstructure into a discoid format. This would then explain the invariance in the DHDAB solution microstructure with concentration. For concentrations exceeding 100 mM, the inability to fit the data to the Nallet model indicates that the bi/multilamellar vesicle model is no longer appropriate. A possible explanation is that the scattering data at 100 mM and above contains additional contributions from an additional mesophase which contributes also to the scattering. Though too weak for this mesophase to be individually identified, there is a sufficiently large contribution to the scattering intensity that the assumption that the scattering is due to the powder average of a single lamellar mesophase is now no longer valid.

Figure 11 shows the κB product derived from the analysis of the scattering data (filled circles).

The data presented show a complex variation in the experimentally derived κB product as a function of solution concentration up to 100 mM. Over a concentration range 1.5−40 mM, the κB values increase with concentration. For the remainder of the concentration range, there is a monotonic decrease in their value with increasing concentration. This suggests that there is a change in either the lamella rigidity or in the compressibility

(53) Douliez, J.-P.; Gaillard, C.; Navailles, L.; Nallet, F. *Langmuir* **2006**, *22*, 2942.
(54) Bryskhe, K.; Bulut, S.; Olsson, U. *J. Phys. Chem. B* **2005**, *109*, 9265.
(55) Jung, H. T.; Coldren, B.; Zasadzinski, J. A.; Lampietro, D. J.; Kaler, E. W. *Proc. Natl. Acad. Sci. U.S.A.* **2001**, *98*, 1353.
(56) Fogden, A.; Hyde, S. T.; Lundberg, G. *J. Chem. Soc., Faraday Trans.* **1991**, *87*, 949.
(57) Soubiran, L.; Staples, E.; Tucker, I.; Penfold, J.; Creeth, A. *Langmuir* **2001**, *17*, 7988.
(58) Freyssingeas, E.; Martin, A.; Roux, D. *Eur. Phys. J. E* **2005**, *18*, 219.

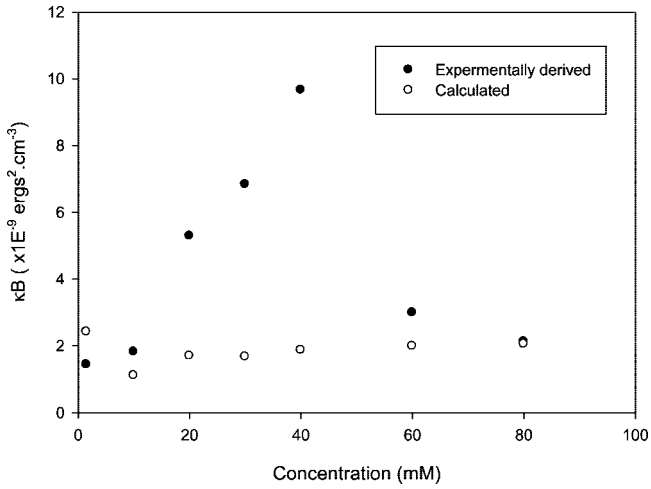

Figure 11. Variation in the κB product as a function of DHDAB solution concentration. The solid circles are the values derived from the fits to the scattering data using eq 18. The open circles are calculated values from eqs 19 and 20.

of the "stack of lamellae", either of which are consistent with a change in the aggregate microstructure.

The previous discussion was based on the approach of Bryskhe et al.[54] and assumed that B was constant and that the change in microstructure (from vesicles to discoids) could be attributed to a change in κ. However, Freyssingeas et al.,[58] Richetti et al.,[59] and Roux and Safinya[60] have assumed, from the variation of η with d, that B varies and κ is constant. However, we can make some estimates of the membrane rigidity, κ, and compressibility, B, for systems stabilized by electrostatics. The magnitude of the membrane rigidity, κ, can be estimated for ionic systems[61,11] as

$$\kappa = \frac{4\varepsilon_D\varepsilon_o}{\kappa_{DH}}\left(\frac{k_BT}{e}\right) \tag{19}$$

Here, e is the electronic charge, ε_D is the dielectric constant of water, ε_o is the permittivity of free space, and κ_{DH} is the inverse Debye−Huckel screening length. For an ionic strength of 1.5 mM, $1/\kappa_{DH} \sim 100$ Å, and κ is approximately $1.5k_BT$. Similarly, assuming that the compressibility is dominated by electrostatics, B may be estimated by[59,60]

$$B = \frac{\pi^2 d k_B T}{2L(d-\delta)^3}\left[1 - 3\frac{\Sigma}{\alpha L(d-\delta)} + 6\frac{\Sigma^2}{\alpha^2 L^2 (d-\delta)^2} + \cdots\right] \tag{20}$$

where α is a dissociation constant (assumed to be ~1.0), Σ is the surface area of the molecule (assumed 60 Å^2), and L is a characteristic length given by

$$L = \frac{\pi e^2}{\varepsilon_D k_B T} \tag{21}$$

and is typically ~20 Å. For d varying from 370 to 850 Å, B varies from 13.1×10^4 to 1.6×10^4 ergs·cm^{-3}. Using eqs 20 and 21, the κB product has been estimated, and the data are shown as open circles in Figure 12. The detailed calculations, together with the variation in κ and B, are shown in section 6

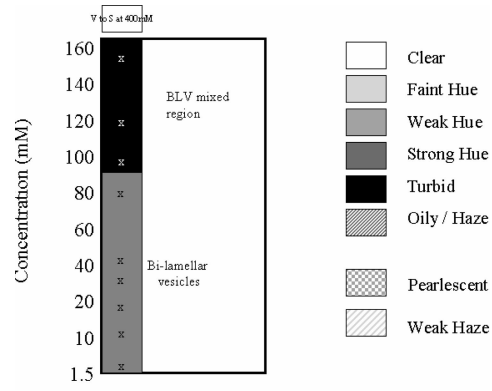

Figure 12. Variation in solution optical texture and phase assignment with solution concentrations for DHDAB solutions at 30 °C.

of the Supporting Information. The calculated κB product is broadly quantitatively consistent with the values derived experimentally from the variation of η with surfactant concentration. However, the detailed variation of κB with surfactant concentration is not predicted. This could be due to the variation in κ and/or B being more complex than is predicted theoretically for this system. This is contrast to the work of Freyssingeas et al.[58] where the absolute scaling was not replicated but the experimental and calculated κB values had the same functional form. There is some uncertainty regarding the actual calculated value of κ, as the electrolyte in the system derives from the free surfactant monomer ($\sim 10^{-4}$ M) and counterion dissociation from the vesicles, and for the purposes of illustration only the assumption is that the surfactant is 100% dissociated. Nevertheless, the magnitudes of κ and B are broadly consistent with literature values, and the variation in B is broadly consistent with the observations of Tsapis et al.,[62] where long-range electrostatic interactions predominantly affect the compressibility, B. It would therefore seem reasonable that changes in both κ and B are required to explain the data in Figure 12 and the observed changes in BLV morphology. Alternatively, the theoretical approach, assuming elastic fluctuations, may not be valid for small numbers of bilayers obtained here.

Figure 12 shows the changes in appearance of DHDAB solution stored at 30 °C as a function of solution concentration together with their phase assignment.

The change in optical texture at high concentration (>100 mM) indicates a change in the solution microstructure and, allied with the inability to apply the Nallet model, suggests that the solution is composed of more than one coexisting mesophase.

The Caille parameters determined using the Nallet model, which is related to the bending rigidity and the compressibility, are relatively low. Caille is typically ~0.07 for solution concentrations 1.5−40 mM, and this indicates highly rigid membranes. This is expected of membranes whose interactions are dominated by electrostatic interactions. Above 40 mM, the value of the Caille parameter increases to 0.2 at 100 mM solution concentration, and above 100 mM it is not possible to adequately model the data using this approach. The membranes are still relatively rigid at this concentration. For comparison, the typical values for aerosol-OT (AOT) and didodecyl dimethylammonium bromide (DDAB)[29] are ~0.15−0.25, and for pentaethylene monododecyl ether ($C_{12}E_5$)[63] they are ~0.3−1.5. The results for the solutions studied here are consistent with previous work on the shear induced transition from lamellar to liposomes in an aqueous dispersion of a similar (commercial) dichain cationic system, Arquad 2HT.[57] This was also characteristic of a rigid

(59) Richetti, P.; Kekicheff, P.; Parker, J. L.; Ninham, D. W. *Nature* **1990**, *346*, 252.
(60) Roux, D.; Safinya, C. R. *J. Phys. (Paris)* **1988**, *49*, 307.
(61) Mitchell, D. J.; Ninham, D. W. *Langmuir* **1989**, *5*, 1121.
(62) Tsapis, N.; Ober, R.; Urbach, W. *Langmuir* **2000**, *16*, 2968.
(63) Yang, B. S.; Lal, J.; Richetti, P.; Marques, C. M.; Russell, W. B.; Prud'homme, R. K. *Langmuir* **2001**, *17*, 5834.

bilayer due to electrostatic stabilization, compared with those stabilized by fluctuations.[63]

5. Summary

DHDAB is more soluble than previously reported,[6,13,41] and close agreement between the experimentally determined values from surface tension and neutron reflectivity yield a mean value of $4 \pm 2 \times 10^{-5}$ M. Slow kinetics of adsorption are observed where surfaces require 3−4 h in order to achieve equilibrium. The inconsistency between the relatively high CAC and the slow surface kinetics is a consequence of diffusion limited processes moderated by slow dissolution of the bulk aggregates. SANS shows that the predominant form of the bulk aggregates is bilamellar vesicles. Using a combination of USANS, PCS, and CryoTEM, the existence of the bilamellar vesicle structure is further confirmed. The predominance of the BLV structure, the absence of any major structural change, and the variation of κB within the concentration range studied are difficult to explain in the context of existing theoretical treatments.

Acknowledgment. The authors are grateful to Dr. E. J. Staples, formerly of Unilever Research Port Sunlight, for fruitful discussions during the course of this work. The TEM images were recorded using the Intertek Northwest facilities at Port Sunlight. We are grateful to the ISIS, ILL, and NIST facilities for the provision of beam time and to the instrument scientists for their support. Certain commercial equipment, instruments, or materials are identified in this paper; this does not imply recommendation or endorsement by the National Institute of Standards and Technology, nor does it imply that the materials or equipment identified are necessarily the best available for the purpose. This research has utilized facilities supported in part by the National Science Foundation under Agreement No. DMR-0454672.

Supporting Information Available: Details of the estimate of phase volume, reproducibility of PCS data, the fit to the USANS data using the core−shell model, and calculations regarding the stability of vesicles relative to discoids. DSC data are included to support the sample preparation methods detailed in the manuscript, and estimates of membrane moduli are also included. This material is available free of charge via the Internet at http://pubs.acs.org.

LA703415M